Available online at www.sciencedirect.com

ScienceDirect

Journal of Energy Storage 00 (2020) 1–26

Journal of Energy Storage

Frequency domain non-linear characterisation and analysis of lithium-ion battery electrodes

C. Fan[a,*], K. O'Regan[b,c], L. Li[a,c], E. Kendrick[b,c], W.D. Widanage[a,c]

[a] *WMG, University of Warwick, Coventry, CV4 7AL, United Kingdom*
[b] *School of Metallurgy and Materials, University of Birmingham, Edgbaston, Birmingham, BT15 2TT, United Kingdom*
[c] *The Faraday Institution, Quad One, Becquerel Avenue, Harwell Campus, Didcot, OX11 0RA, United Kingdom*

Abstract

As an electrochemical system, the current voltage relationship of a lithium-ion battery is non-linear. The accuracy of conventional models for lithium-ion cells always suffer from non-linear dynamic behavior, especially at low SoC levels and high current levels, which limits practical applications of battery models in reality. In-depth understanding and characterisation of the non-linear relationship can provide valuable insight to improve the accuracy of battery modelling. In this paper, a frequency domain non-linearity characterization approach using odd random-phase multisines signals is performed on a three-electrode experimental set-up of a commercial 5Ah cylindrical 21700 cell. This allowed the distortions towards the full-cell voltage to be separated into the corresponding electrodes and identify the nature of non-linearity as odd or even order. The results demonstrate that the even order non-linearity from the cathode is the main contributor towards the full-cell voltage of the lithium-ion battery while the non-linearity from the anode starts to dominate at very low (~ 2%) state-of-charge.

Keywords:
Lithium-ion battery, Non-linear characterisation, Random phase odd multisine signals, Odd-even distortions, Three-electrode cell

1. Introduction

Nowadays, lithium-ion batteries are widely utilized as energy storage systems in new-energy vehicle applications, like electric vehicles (EV) and hybrid electric vehicles (HEV). To effectively control batteries under various operating situations, a comprehensive and reliable battery management system (BMS) is indispensable. Critical but unmeasurable variables and battery states, such as core temperature, state of charge (SOC) and state of health (SOH), can be accurately estimated by advanced model-based estimation algorithms [1–7]. The reliability of these model-based algorithms depends on the accuracy of current voltage responses of battery models. Therefore, accurate battery models play a significant role in the rapid development of contemporary automotive industry.

*Corresponding author
Email address: Chuanxin.Fan@warwick.ac.uk (C. Fan)

In term of battery responses, the change in terminal voltage can be approximately proportional to the change in excitation current at low current levels and high SoC levels, which indicates that the battery system behaves linearly [8]. Many models are designed for these mild working regimes to imitate the current and voltage relationship with equivalent circuit components. In [9], twelve equivalent circuit models (ECM), such as simple lumped models, resistance-capacitance (RC) network based ECM, and RC model with hysteresis, were reviewed and compared. Although ECM can mimic battery input and output response behavior, the equivalent circuit structure with fixed parameters is a linear system relating current to voltage thus any non-linear behavior of a battery is neglected. But, as widely known, in the case of low SoC levels, the current voltage relationship is not linear which implies that the non-linearity of a lithium ion battery is significant, and it thus results in poor model accuracy [10]. Then some ECM with variable parameters are designed to provide better fidelity [11], however, the precision at low SoC level was rarely considered. This limits the optimal SoC window of a Li-ion battery between around 10% and 90% in practice by EV manufacturers [12]. Therefore, improving the accuracy of models at low SoC is essential to maximize the energy utilisation of a battery. By interpreting the electrochemical behaviors in the electrodes and electrolyte, electrochemical models have been proposed to achieve high accuracy in recent years such as the pseudo-two-dimensional (P2D) model [13], single particle model (SPM) [14], and single particle model with electrolyte (SPMe) [15]. However, electrochemical models require many parameters and involve coupled partial differential equations, and the heavy calculation burden can also restrict the practical applications. To ensure high model accuracy under extreme conditions, the non-linearity part of a model has to be taken into account [16]. Therefore, a current challenge is how to simultaneously cover the description of a battery's non-linear behavior to maintain high accuracy over a wide SoC condition, while maintaining the simplicity of model. In order to achieve this goal, in-depth understanding of battery non-linearity and its related sources are important to improve the accuracy of battery modelling.

The dynamic behavior of a battery is due to electrochemical processes such as charge transfer kinetics, mass transport, and thermodynamics [16]. Mathematically, Butler-Volmer equation is utilized to represent the charge transfer kinetics on electrode and electrolyte interface, and a diffusion process according to Fick's law is applied to account for mass transport [17, 18]. Since the non-linearity of a battery system is practically caused by multiple coupled processes, a pure model-based analysis with assumptions cannot truly describe all the responses. Therefore, an experiment based analysis is still necessary, and the non-linearity must be effectively characterized, which is the focus of this paper.

Frequency domain approaches with well-designed excitation harmonics can provide essential information, such as non-linearity, for characterizing battery behavior. Because of these advantages, many investigations in the frequency domain, like Electrochemical Impedance Spectroscopy (EIS) and Non-linear Frequency Response Analysis (NFRA), have been made for Li-ion battery characterization [19, 20]. The EIS technique is achieved by exciting successive single sine sweep signals for battery characterization. EIS can be widely employed to investigate the fundamental battery states, like state of health (SoH) and state of charge (SoC), over a wide frequency range from milli-Hertz to mega-Hertz [21]. The swept sine approach of sine-waves leads to very time consuming testing for low frequency

experiments. On the other hand, EIS limits analysis to linear frequency responses only. However, as an electrochemical energy system, strong non-linear processes occur in Lithium-ion batteries at high current input signal, such that the characterization of non-linearities cannot be neglected [16]. In order to extend dynamic analysis from linear to non-linear level, Harting et al. first applied Non-linear Frequency Response Analysis (NFRA) techniques on lithium-ion batteries by increasing amplitude of AC excitation to the weakly non-linear regime. In [20], the non-linear contribution of solid diffusion, reaction and ionic transport was characterized, respectively. Additionally, C-rate and temperature dependency of battery non-linear responses were studied as well. Wolff et al also present a model based analysis via NFRA technique to understand and interpret the excitation of higher harmonics, and the impact of parameter variations on non-linearity [18]. Although NFRA can provide comprehensive analysis of battery behavior, the protracted measuring time is, however, still an obstacle to practical applications in real life. In recent years, based on system identification theory, some preliminary studies have been proposed for fast Li-ion battery characterization with different excitation signals in frequency domain analysis [22–26]. The authors of [22] designed and performed multisine excitation signal as a fast characterization technique to gather impedance information, however, the research only focuses on the linear behavior of battery. Widanage et al proposed a new signal designed technique, named as pulse-multisine, which can effectively capture the non-linear behavior of a Li-ion battery [23]. Unfortunately, the battery system non-linearity was not explicitly analysed in that study. Focusing on non-linearity analysis of battery, the authors of [26] applied random phase multisine signals with multiple realizations for battery dynamics detection which allows separating non-linear distortion and noise disturbance from the linear part of battery. The excitation signals can also require a short testing time in comparison with conventional single sine sweep measurements (EIS and NFRA). However, multiple signal realizations for characterizing random phase non-linear distortion will prolong the testing duration and increase computation of signal design procedure. Thus, an efficient non-linearity characterization approach, which considers both linear and non-linear behaviors, is crucial to provide necessary information of battery behavior.

Additionally, in all the aforementioned studies, the research is typically based upon voltage measurements of full cells with different chemistries, as a result the voltage response is not decoupled to the electrochemical processes taking place at individual electrodes. The contribution of non-linearity has not been determined between anode and cathode by conventional full cells, and therefore requires the intervention of novel technique to de-convolute the electrochemical behaviors of the individual electrodes. In literature, this is often done using half-cell configurations, but the use of a lithium metal counter electrode means the behavior does not closely resemble the commercial battery [27, 28]. Here, we chose a three-electrode configuration to more closely resemble a commercial cell making the conclusions more relevant to practical applications [29–32]. In [29], the insertion method with a pure metallic lithium reference electrode enables direct observation of voltage responses of the individual electrode. Moreover, for assigning the entire cell behavior into individual electrodes, Wunsch et al proposed an experimental method to depict the separation of individual electrodes through impedance spectra [32]. To our best knowledge, the analysis of non-linear voltage responses observed at a full cell stage as well as individual electrodes via three-electrode arrangements has

not been studied.

1.1. Contribution of the paper

A multi-frequency signal is designed to investigate the level of non-linearity in the frequency domain. Further, this study detects and qualifies the linear dynamics, non-linear distortion and noise disturbance not only of a full cell, but also individual electrodes. The non-linear distortion gives a new perspective in understanding battery behavior. The proposed frequency domain method allows the non-linearity to be grouped into odd and even contributions which could provide valuable information for the system non-linear part modelling, and the dominant contributor between cathode and anode is investigated. Plus, a specific case, which presents significant non-linear response at 2% SoC level, is also discussed.

1.2. Organization of the paper

In Section 2 of this paper, the design of random odd multisine signals is explained and the characteristic frequency range of the anode and cathode is shown by potentiostatic electrochemical impedance spectroscopy (PEIS) in a three-electrode cell. The experiment setup for the three-electrode cell is introduced in Section 3, including the frequency range selection and random harmonics suppressing procedure, and also the measured current signal and voltage response of the cell are evaluated. In Section 4, the theory of non-linear distortion on the voltage response spectrum is presented, and the frequency response function (FRF) of a system, which composes of best linear approximation, non-linear and noise distortion, is identified by a fast frequency domain approach. In Section 5, the frequency domain analysis is performed on EL-Cells, and the frequency spectrum are analysed and discussed.

2. Random phase odd multisine signal

In this section, the random phase odd multisine is introduced as a current signal for non-linear characterisation. Furthermore, the characteristic frequency range of each electrochemical process of EL-Cell is presented for the frequency range selection of the designed multisine signals.

2.1. Random phase multisine signals

Unlike a single sine sweep in conventional EIS, multisine signals are periodic broadband signal which are formed by the superposition of multiple sinusoidal waves with different frequencies. Due to the superposition feature, a multisine signal can scan a wide frequency range within one period, which results in a significant reduction in experiment time. The expression of a general multisine excitation signal is as Eq.(1).

$$u(t) = \sum_{n=1}^{N} A_n \cos\left(2\pi f_n t + \varphi_n\right) \qquad n = 1, ..., N \tag{1}$$

Where t is time, N is the number of excited frequencies, f_n is the nth excited frequency, A_n is the amplitude and φ_n is the phase of f_n. By Discrete Fourier transform (DFT) and inverse Discrete Fourier transform (iDFT) techniques, the excited frequencies of multisine can be designed by inserting excited harmonics at corresponding frequencies f_n in frequency domain. The non-excited frequencies, named detection frequencies, can be utilized to detect the non-linear distortion of the system under examination. The highest frequency f_{max} of a multisine signal could be freely chosen, however, by Shannon sampling theorem, the upper bound of f_{max} must be set to less than half the sampling frequency f_s. The sampling frequency f_s is generally restricted by software or hardware limitation. Moreover, because of adding several sinusoidal waves for multisines, the lowest frequency f_{min} will determine the length of signal duration T for one single period. Therefore, the total length will be $T \times P$ if the signal is repeated P times for the periodical excitation signal. Furthermore, in multisine signal design, the amplitude A_n and phase φ_n of all excited frequencies can be free set by the user for a specific application. The resulting signal is then known as random phase multisine. It is subsequently normalised by its root mean square (rms) and multiplied by the desired rms for a given experiment.

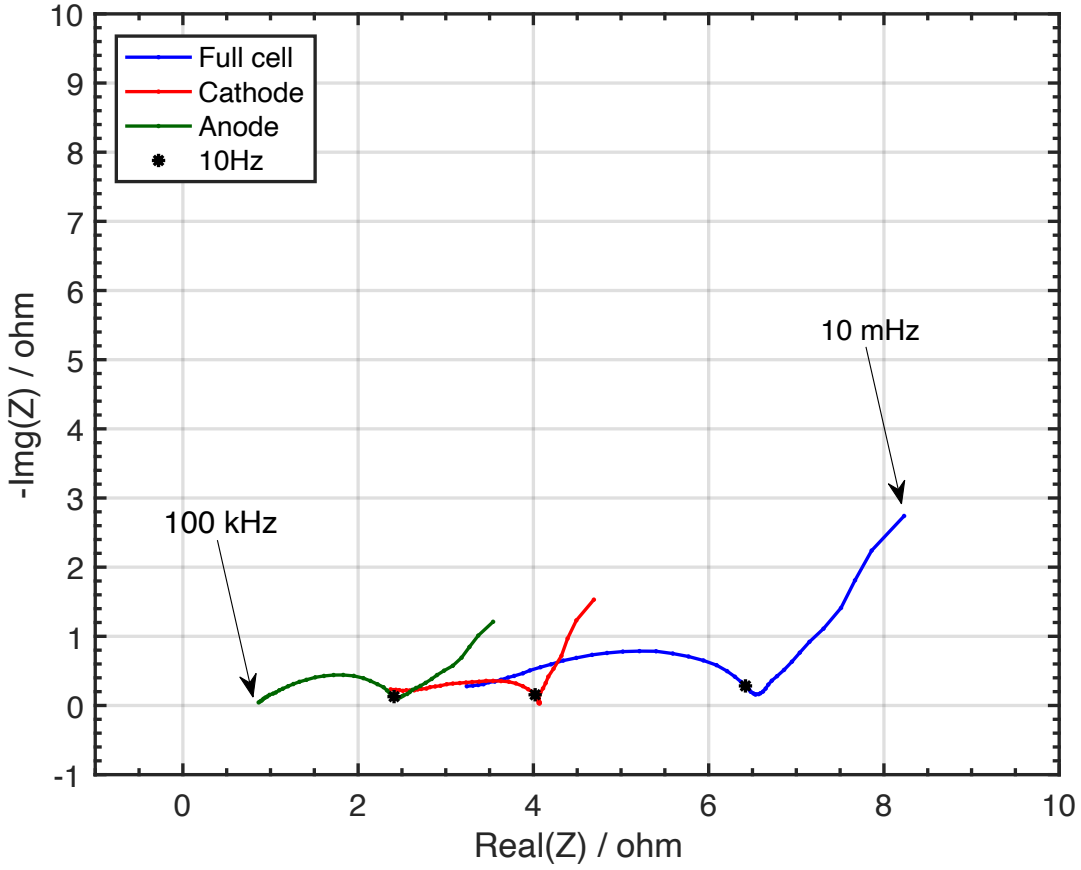

Fig. 1. PEIS Nyquist plot of the NMC EL-Cell at 50% SoC. Note that the frequency range of PEIS was from 10 mHz to 100 kHz.

2.2. Characteristic frequency range of EL-Cell

In this study, the design parameters of the multisine signals for a three-electrode EL-Cell were determined by considering the following aspects: battery dynamic response, hardware/software limitation, safety concerns and specific objective [26].

Theoretically, the dynamic response of a lithium-ion battery is governed by mass transport processes, thermodynamics, and charge-transfer kinetics [16]. In the frequency domain, the characteristic frequency ranges of the particular governing processes are distinct: for instance, Harting et al concluded that, for a NMC pouch format cell in [20], the low frequency range from 0.02 Hz to 1 Hz is for thermodynamics and diffusion processes, the medium frequency range from 1 Hz to approximately 200 Hz is for porous electrode reactions, such as double-layer capacitance and charge transfer kinetics, and the high frequency range is for faster processes such as ionic transport, such as migration, between SEI and electrolyte from approximately 200 Hz and 10 kHz. However, in this study, the experimental cell is a three-electrode configuration experimental cell known as PAT-Cells (EL-Cell), and the instrument configuration causes an increase in cell impedance, which leads to distinct characterization frequency ranges. To determine the characteristic frequency range of EL-Cell, the PEIS was firstly performed on the considered EL-Cell at 50% SoC, and the measured impedance spectra of cathode, anode and full cell are shown in Fig.1. In the PEIS experiment design, the AC perturbation signal was limited to 10 mV for minimizing non-linear effects, and also the PEIS frequency range was controlled between 10 mHz and 100 kHz.

In Fig.1, the measured impedance can be divided into two distinct parts for low frequency range 10 mHz to 4 Hz and a semi-circle for medium frequency range 4 Hz to 100 kHz. As mentioned above, the low frequency range represent the frequency response of diffusion process and the medium frequency range corresponds to electrode reactions. In general, at 100 kHz and above the EIS plot of a commercial cell format (rather than an EL-cell) would surpass the real axis [19, 21, 33]. However, no such response is present in any of the impedance spectra of Fig.1. The reason is the low inductive internal structure caused by the three-electrode cell configuration. The reason is the low inductive internal structure caused by the three-electrode cell configuration and the optimized voltage measurement and contacting of the EL-cell [32]. In addition, due to the uneven current distribution within the cell, the three-electrode configuration measurements with reference electrode could show artefacts, such as inductive loop [34]. However, in this study, the PEIS results demonstrate only trivial artefacts in the cathode, which is acceptable for further analysis. Further, the impedance value of the anode is lower than the cathode at the same frequency. In the anode spectrum, the impedance at the highest frequency almost reaches the real axis, which is commonly considered as the beginning of the high frequency part of lithium ion battery impedance. However, the impedance at the same frequency of the cathode spectrum is still in the semi-circle of the medium frequency range. These phenomena is consistent with [32], and it can be interpreted due to the higher electrical resistances of the cathode NMC than the anode graphite material.

3. Experiments setup and measurements

The experiment was conducted using a three-electrode configuration to allow deconvolution of the cathode and anode behaviors from the full cell potential. PAT-Cells (EL-Cell) were comprised of a 21.6 mm FS-5P separator (EL-Cell), 100 µl of R&D281 electrolyte (Soulbrain), and the extracted positive electrode and negative electrodes punched into 18 mm disks. The electrodes (anode/cathode) were harvested from a fresh 21700 LGM50 cylindrical cells following the reported teardown procedure [35]. Note the fresh cylindrical cells are purchased from the manufacturer and stored in a fridge (5 $^{\circ}C$) until they were discharged to 2.5 V and then disassembled. The reference electrode purchased from EL-Cell is comprised of a stainless steel ring that had lithium metal deposited on it. The extracted $NMC811$ cathode and bi-component $Graphite - SiO_x$ anode had the coating on one-side removed to allow testing in a small format cell. Furthermore, the composition of Soulbrain R&D281 is ethylene carbonate(EC):ethylmethyl carbonate(EMC) 3:7 v/v + 1 wt% vinylene carbonate(VC). The nominal rated capacity of EL-Cell in this study was 11.5 mA h, which also decides the magnitude of the 1 C-rate (1C) as 11.5 mA.

Before the multisine signals were applied to the assembled cells, a formation protocol was used to ensure that the solid electrolyte interphase (SEI) had reformed. Extraction of the electrodes and using a different electrolyte meant this step was required to ensure cell longevity. This formation protocol consisted of two cycles at C/10 constant current constant voltage (CC-CV) charge and constant current (CC) discharge between the recommended voltage window 2.5-4.2 V. The CV step was terminated when the current decayed to C/50. The signals were programmed using the 'Batch Mode' function in the EC-Lab software (Bio-Logic®).

Table 1
Test matrix of studied multisines experiments for EL-Cells at ambient temperature 25 °C. Tested combinations of SoC and C-rate are marked by an 'x' for 10 periods and an '△' for 20 periods.

SoC	**C-rate**				
	0.2C	0.5C	1.0C	1.5C	2.0C
2%	△	△	△	△	△
10%	x	x	x	x	x
50%	x	x	x	x	
90%	x	x	x	x	

Once the formation cycles were complete, multisine signals were applied over a wide range of SoCs and C-rates as given in Table 1. This study focuses on the frequency dynamic response of the diffusion process and the electrode reaction of lithium-ion battery full cell and individual electrodes. As mentioned in the last section, the low characteristic frequency range of EL-Cells (10 mHz to 4 Hz) must be covered for the diffusion process. Furthermore, referring to [18], the model based analysis result shows that, when the electrode reaction varies, the magnitude of non-linear distortion in the medium frequency range will change accordingly but the energy at all frequencies remains the same value. Therefore, the frequency range of 4 Hz to 10 Hz was selected for describing electrode reaction

dynamics. Consequently, the excited signal frequency range in this study was determined from 10 mHz to 10 Hz. Thus, the resulting signal period T is 100 s according to the minimum frequency of 10 mHz. Since the influence of measurement noise and transient effects can be minimised to classify and quantify the non-linear distortions by using period signals, the total number of periods used at a given SoC is 10 and the experiment duration per SoC is therefore 1000 s. To ensure the signals are stable and reproducible, in this work, we designed one single period signal for each C-rate and repeated it for preset number of periods, which can minimize the input difference between individual periods. The sampling frequency f_s was fixed as 50 Hz to accurately capture the full frequency range and minimise signal aliasing.

After determining the frequency range, random phase odd multisines were designed for detecting non-linear distortions by suppressing specific harmonics in the frequency domain. Firstly, in the multisines, the fundamental frequency, which is 0 harmonic, was suppressed for obtaining the zero-mean current signal to ensure the cells' steady state. And then, to eliminate all non-linear interaction from even harmonics, all even harmonics within the considered frequency range of the designed current signal are suppressed. Furthermore, in order to reduce the non-linear interaction from odd harmonics for best linear approximation and arbitrarily characterize non-linearity, some odd harmonics are suppressed by dividing all odd harmonics into three per group and randomly suppressing one harmonic from each group [36]. These suppressed harmonics are termed as detection harmonics, since the level energy that appear in these harmonics are examined in the output voltage response. Therefore, in this work, a total 334 odd harmonics were excited as $k = 1, 5, 7, 9, 13, 15, 21, 23, ..., 999$ for all C-rate signals, and the amplitudes are identical across all the excited harmonics (a flat spectrum) and that the phase is a uniformly distributed random variable between 0 to 2π. By applying the designed odd multisine signals, the energy appearing at the suppressed even harmonics in the voltage spectrum are due to even order non-linear distortions and the energy appearing at the suppressed odd harmonics are due to odd order non-linear distortions [26, 36].

The designed multisine current signals were applied to fresh EL-Cells and the rms amplitude of the multisine signals were set as 2.3 mA, 5.75 mA, 11.5 mA, 17.25 mA, and 23 mA, corresponding to 0.2C, 0.5C, 1.0C, 1.5C and 2.0C, respectively. In addition, each input signal was repeated at different SoC levels (2%, 10%, 50%, and 90%) for all EL-Cells (see Table 1). The state of charge (SoC) is defined exclusively by the discharge voltage. This is to avoid SoC uncertainty caused by voltage hysteresis and cell capacity variations. To attain the desired SoC, the cell is charged to 4.2 V at $C/10$ CC-CV (C/50 cut-off), then discharged at $C/10$ constant current, via predetermined voltages, to each of the desired SoCs in descending order, i.e. 90% - 50% - 10% - 2% SoC, as in Fig.2 shown.

The 2.0C multisine signal at 50% and 90% SoCs resulted in large voltage drops associated with the high current being applied and the anode voltage dropped below 0 V during experiments which indicates lithium plating on the anode [37]. These two operating conditions were therefore excluded from the investigation as to prolong cell longevity and avoid unwanted effects caused by lithium plating. In addition, it was also observed that, at 2% SoC, the dynamic voltage response of a EL-Cell did not reach a steady-state behavior within 10 periods, thus, the testing was extended to 20 periods from 10 periods for further analysis as a special case.

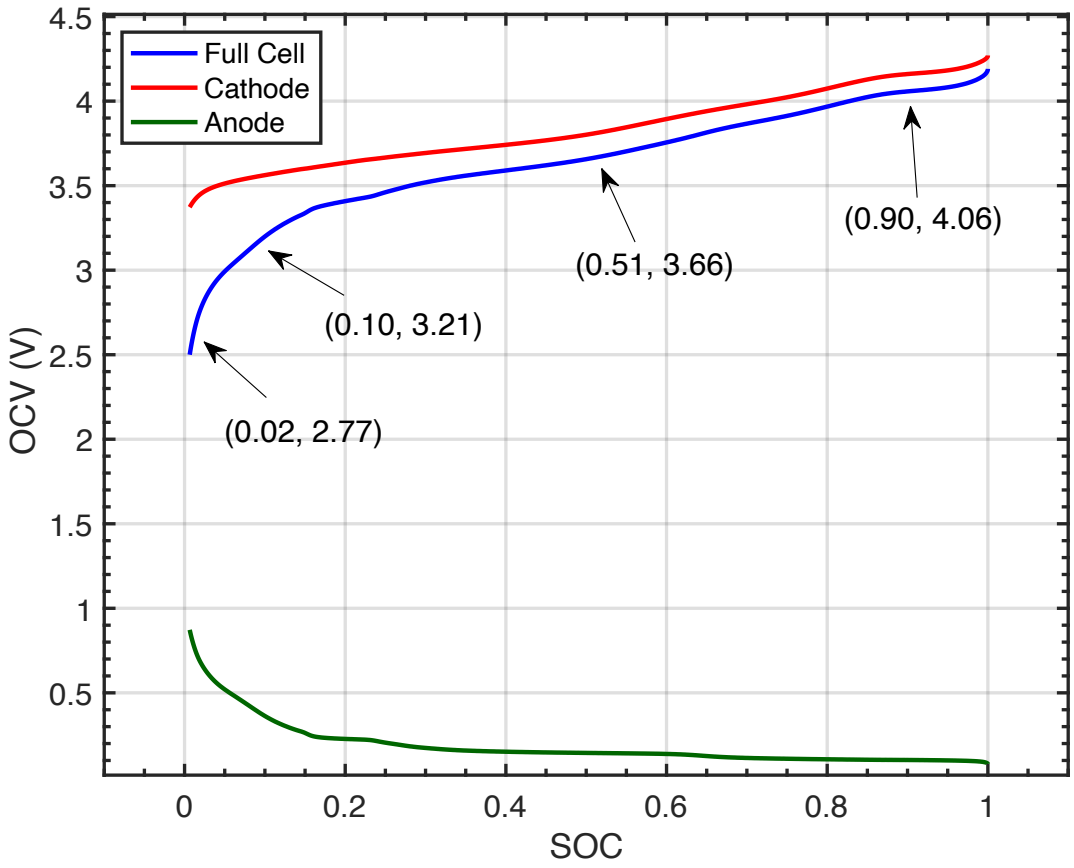

Fig. 2. Discharge voltage profiles for the anode, cathode and full cell. Annotations illustrate the voltages that correspond to the SoCs 2%, 10%, 50%, and 90%

As an example, Fig.3 presents the averaged (averaged over the 10 periods) measured data of input current and voltage response at 0.2 C-rate and 90% SoC. The positive current value implies the charge process in Fig.3(a) and negative current for discharge. Furthermore, the error between the measured current and the designed signal is shown in Fig.3(b) which indicates the current signal generated by the Biologic VMP3 hardware is not perfect and the analysis needs to account for this signal generator disturbance (as explained in Section 4.2). In this manuscript, all experiments in this study were conducted in a thermal chamber at room temperature (25°C) and the SoC variation due to the multisine experiment was estimated by Coulomb counting [38]. It shows that a 0.01% SoC change occurs over a given period for 0.2 C-rate testing, refer to Fig.3(b), and a maximum of 1% SoC change for all other experiments. Based on these values the SoC can be treated as a constant during the analysis.

The voltage response should reach a steady-state behavior for the subsequent analysis. For the calculation of transient error, the measured voltage of the last period of each experiment was considered as the benchmark, and the transient error was obtained by comparing the voltage response against the previous periods. In this study, after the

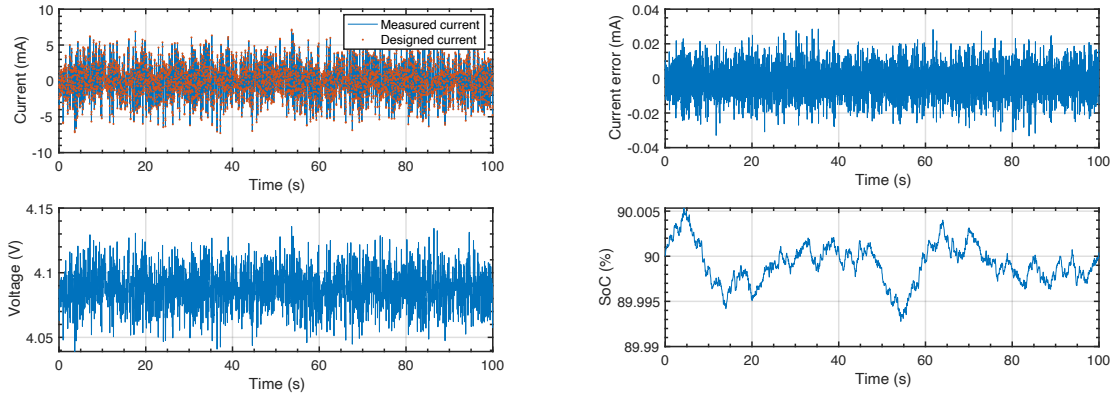

(a) (b)

Fig. 3. One period (averaged over the periods) of the measured current and voltage data at 0.2 C-rate 90% SoC: (a) averaged measured current and voltage, (b) averaged measured current error and estimated SoC.

first 3 periods, the testing system can be considered to have fully passed through the transient stage. Therefore, the first 3 periods were excluded from all datasets in the following data analysis processes to ensure the transient error can be neglected, except for 2.0% SoC experiments which requires 20 periods to reach steady state and the first 13 periods were eliminated for analysis. Note that since the input current was designed as zero-mean signal, the steady-state will be kept once the cell system passes through the transient stage. Therefore, the inconsistent number of periods will not have a significant effect on the data interpretation.

In the next section, the theory of non-linearity characterization in the frequency domain is presented. Moreover, the non-linear distortion of a full cell, cathode and anode, and the influence of current level and SoC level will be discussed.

4. Frequency domain analysis

Fig.4 illustrates the representations of a lithium-ion battery system, which is driven by noisy input, in both time domain and frequency domain. In practical, the input and output measurements data are recorded as discrete data points in time domain which can be noted as:

$$u^{[p]}(n), \quad y^{[p]}(n) \qquad p = 1, 2, ..., P \qquad n = 0, 1, ..., N-1 \tag{2}$$

Where p indicates the pth period of the input signal $u(n)$ and of the output voltage response $y(n)$. In Eq.(2), N is the number of samples per period of the applied multisine. The pth period measured input signal $u^{[p]}(n)$ consist of the designed signal $u_0^{[p]}(n)$ and equipment noise $n_u^{[p]}(n)$. Then, by fast Fourier transform (FFT), the discrete time domain

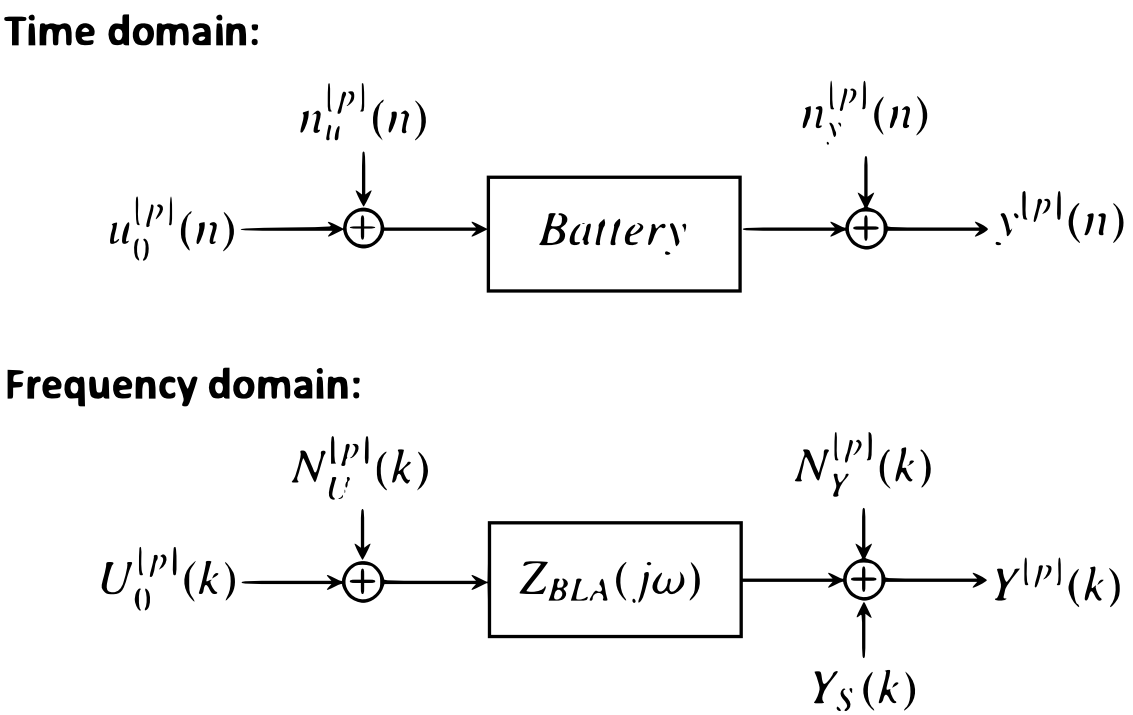

Fig. 4. The time domain and frequency domain representations of a battery system driven by noisy input.

data can be transformed to frequency domain, termed as input and output spectra of pth period:

$$U^{[p]}(k), \quad Y^{[p]}(k) \qquad k = 0, 1, ..., N-1 \tag{3}$$

where $U^{[p]}(k)$, $Y^{[p]}(k)$ in Eq.(3) denote the DFT of $u^{[p]}(n)$, $y^{[p]}(n)$ at the kth harmonic.

In the frequency domain, the spectra of measured input/output data can be represented as:

$$\begin{aligned} U^{[p]}(k) &= U_0^{[p]}(k) + N_U^{[p]}(k) \\ Y^{[p]}(k) &= Z_{BLA}(j\omega) \times U^{[p]}(k) + Y_S(k) + N_Y^{[p]}(k) \end{aligned} \tag{4}$$

Where $U_0^{[p]}(k)$ represents the ideal designed multisine signal, $Z_{BLA}(j\omega_k)$ is the frequency response function (FRF), termed as best linear approximation (BLA) of the battery impedance, $j\omega$ is the complex frequency variable, $Y_S(k)$ characterizes the non-linear distortion, and $N_U^{[p]}(k)$ and $N_Y^{[p]}(k)$ indicate the noise distortion from practical environment and measurement hardware in the input and output spectrum, respectively.

In the following sections, the calculation of the non-linear distortion and noise distortion on the voltage response spectrum will be presented. Further, the manuscript introduces how the frequency response function (FRF) of the

battery impedance and the noise standard deviation can be detected by analysis the multiple periods.

4.1. Non-linear distortion on voltage response spectrum

Based on the p periods of measured input/output spectra $U^{[p]}(k)$, $Y^{[p]}(k)$, $p = 1, 2, ..., P$, the average spectra $\hat{U}_{(k)}$, $\hat{Y}_{(k)}$ and the corresponding variances $\sigma^2_{\hat{U}_{(k)}}$, $\sigma^2_{\hat{Y}_{(k)}}$, $\sigma^2_{\hat{Y}_{(k)}\hat{U}_{(k)}}$ at all harmonic k can be calculated, as shown in Eq.(5). Note that the periods p here means the measured periods once the transient periods have been removed (See Section 3).

$$\hat{U}(k) = \frac{1}{P}\sum_{p=1}^{P} U^{[p]}(k) \tag{5a}$$

$$\hat{Y}(k) = \frac{1}{P}\sum_{p=1}^{P} Y^{[p]}(k) \tag{5b}$$

$$\hat{\sigma}^2_{\hat{U},n}(k) = \sum_{p=1}^{P} \frac{\left|U^{[p]}(k) - \hat{U}(k)\right|^2}{P(P-1)} \tag{5c}$$

$$\hat{\sigma}^2_{\hat{Y},n}(k) = \sum_{p=1}^{P} \frac{\left|Y^{[p]}(k) - \hat{Y}(k)\right|^2}{P(P-1)} \tag{5d}$$

$$\hat{\sigma}^2_{\hat{Y}\hat{U},n}(k) = \sum_{p=1}^{P} \frac{(Y^{[p]}(k) - \hat{Y}(k))\overline{(U^{[p]}(k) - \hat{U}(k))}}{P(P-1)} \tag{5e}$$

Theoretically, when an input signal with a frequency ω is applied to an ideal linear system, the output response signal will retain the same frequency but obtain a different amplitude and phase. However, in a non-linear system, inter modulation of the input signal frequencies leads to additional frequency components in the output spectrum. Furthermore as described in Section 3, by having all even harmonics suppressed and several odd harmonics suppressed, the distortions that occur on the suppressed even and odd harmonics of the voltage spectrum are due to even and odd order non-linearities. Thus, the non-linear distortion in the voltage response spectrum can provide essential knowledge about the form of battery non-linear behavior. In this study, since the randomly selected odd $k_{Non,odd}$ and even harmonics $k_{Non,even}$ had been suppressed, the energy at these corresponding harmonics $\hat{Y}(k_{Non,odd})$ and $\hat{Y}(k_{Non,even})$ in the voltage spectrum can be considered as non-linear distortion, which can be utilized to describe non-linearity of a battery system. In addition, the variances $\sigma^2_{\hat{U}_{(k)}}$, $\sigma^2_{\hat{Y}_{(k)}}$ are the level of noise power caused by environment and

measurement.

4.2. Frequency response function (FRF) and distortions detection

The battery impedance $\hat{Z}_{BLA}(j\omega_k)$ (as a best linear approximation (BLA)) at the excited harmonics ω_k can be calculated as Eq.(6):

$$\hat{Z}_{BLA}(j\omega_k) = \frac{\hat{Y}(k)}{\hat{U}(k)} \tag{6}$$

Ideally the energy at the non-excited harmonics of the voltage signal should be due to non-linear distortions. However as the signal generator distorts the suppressed harmonics of the designed multisine current signal (see Fig.3 and Fig.4), the linear contributions of these distortions $\hat{U}(l)$ should be removed from the output spectrum to evaluate the level on non-linear distortion. Thus, once the impedance $\hat{Z}_{BLA}(j\omega_k)$ at the excited harmonics is obtained by Eq.(6), the impedance at the non-excited harmonics ω_l is calculated by interpolating between the nearest excited harmonics ω_k and ω_m, as following Eq.(7).

$$\hat{Z}_{BLA}(j\omega_l) = \frac{(m-l)\times\hat{Z}_{BLA}(j\omega_k) + (l-k)\times\hat{Z}_{BLA}(j\omega_m)}{m-k} \tag{7}$$

The non-linear distortion level in the voltage response can now be quantified by deducting the linear contribution from the distortions of the signal generator as shown in Eq.(8):

$$\hat{Y}_c(l) = \hat{Y}(l) - \hat{Z}_{BLA}(j\omega_l)\times\hat{U}(l) \tag{8}$$

By the theory described in this section, the even and odd non-linear distortion can be separated in the measured output voltage spectrum. The advantage of this approach is the simplicity in the signal design and experiment implementation, since only one realisation is required for this approach for one specific experiment. In the following section, the non-linear distortion will be characterized for a full cell and individual electrodes in an EL-Cell. The behavior of each electrode can be quantified and analysed, which helps to understand the internal behavior of lithium-ion batteries at various operating conditions.

5. Results and discussions

In this section, the frequency domain analysis is performed for the multisine input current and output voltage measured data of the full cell and individual electrodes of the three electrode EL-Cell. Furthermore, the electrode

responsibility for the non-linear distortions observed at the full cell voltage is studied at different SoC levels and excitation current levels.

5.1. Multisines current input spectrum

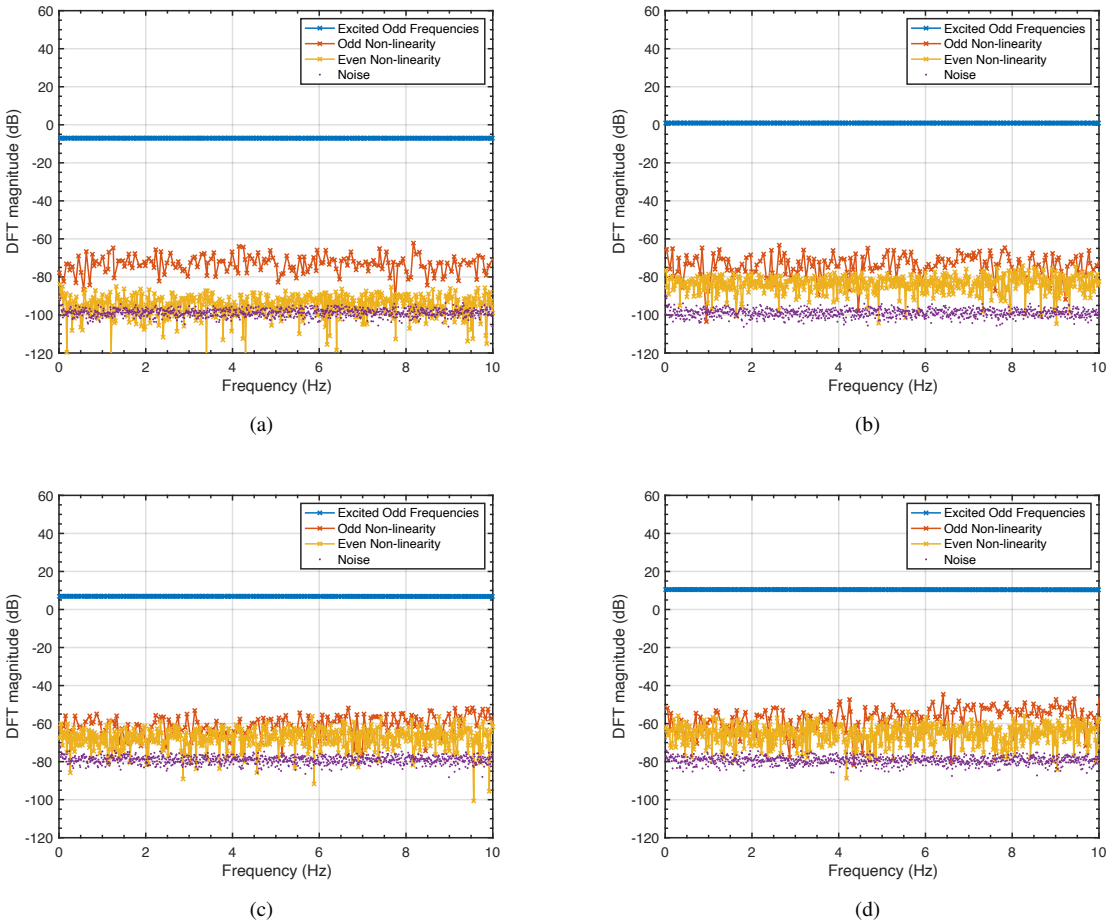

Fig. 5. Current input spectrum while C-rate is: (a) 0.2C, (b) 0.5C, (c) 1.0C and (d) 1.5C

In Fig.5, the spectrum of measured current signals for all SoC levels is shown in the frequency domain. It shows the flat spectrum of the excited harmonics, the signal generator disturbances at the non-excited odd and even harmonics and standard deviation of the noise level. The measured current signals, as designed in Eq.(1), have a flat amplitude spectrum over the excited odd harmonics within 10 mHz to 10 Hz for 0.2C, 0.5C, 1.0C and 1.5C, respectively. Furthermore, the noise spectrum, which is calculated by Eq.(5c) in Section 4.1, is around 90 dB lower than the excited frequencies spectrum. It indicates that the trivial noise doesn't impact the non-linearity characterization, which can be ignored in the following analysis. Note that the MATLAB® function *dB* was used to calculate the magnitude of energies in this study. As mentioned in Section 3, the input current signal is designed with all even harmonics

suppressed and several odd harmonics suppressed. However, the VMP3 signal generator, in practice cannot generate a near perfect current signal as desired and this distorts the harmonics content in the generated or measured current signal and adds energy into the non-excited harmonics that should ideally be zero. The separation of the energy (in the measured current signal) into even and non-excited odd harmonics indicates the nature of non-linearity the signal generator introduced at the expected harmonics. Furthermore, in comparison to the energy measured in the excited harmonics the non-linear distortions (odd and even) are low and shift upward as the amplitude of the excitation signals increase. The error between the designed current and the measured current signal, as shown in Fig.3(b), is composed of both noise and unexpected energy at non-excited harmonics. Because of these distortions a correction must be made when evaluating the level of non-linear distortion in the output spectrum as explained in Section 4 by Eq.(8).

5.2. Non-linear distortions in the voltage response spectrum

In this section the non-linear distortions of the voltage responses (full cell, anode and cathode) are investigated. Starting with the full cell voltage, the distortions are analysed across the different SoCs and C-rates. The distortions are also separated into odd and even distortions to evaluate if a particular form of non-linearity is prevalent in battery dynamics. Finally the anode and cathode distortion levels are studied to identify if and which electrode contributes to the overall non-linear battery behavior.

5.2.1. Dominant non-linear distortion Analysis - Full cell

Fig.6 presents the voltage spectrum at the excited harmonics, the level of distortions at the non-excited harmonics and the standard deviation of the noise of the full cell at 1.5 C-rate current input and different SoC levels (90% SoC, 50% SoC, 10% SoC and 2% SoC). The results show that the magnitude of non-linearity at low SoC levels, such as 10% SoC and 2% SoC, is larger than at higher SoC levels, and the maximum difference of even non-linearity almost reaches −40 dB from 2% to 90%. The non-linearity evolution is therefore consistent with the OCV profile of battery in Fig.2, which also illustrates that the battery at lower SoC levels show stronger non-linear behavior. Furthermore, Fig.6 shows that there is no clear separation of even and odd non-linearities within the frequency range when at 90% and 50% SoC, but a clear separation between odd and even distortions can be found at 10% and 2% SoC, and the amplitude of the even order distortion is larger than the odd order distortion. At 10% SoC, the separation is only noticed during the low frequency range and are of similar magnitude in medium frequency range, however, at 2% SoC, the separation is clear over the whole testing frequency range. Moreover, contrary to the flat noise distortion floor in the other SOC levels, the noise standard deviation at 2% SoC shows a downward slope-type curve, which gradually decreases from −10 dB to −30 dB, indicating some non steady-state behavior in the voltage response.

Based on the non-linear behavior at 10% SoC level, Fig.7 shows the variation of the full cell voltage spectrum when the input current level increases from 0.2 C-rate to 1.5 C-rate, which indicates the effect of C-rate on non-linear distortion. At 0.2 C-rate, both even and odd non-linearities are around the noise level, which means the EL-Cell was performing linearly. When the current level increases, the non-linearities shift upwards and separate from noise floor.

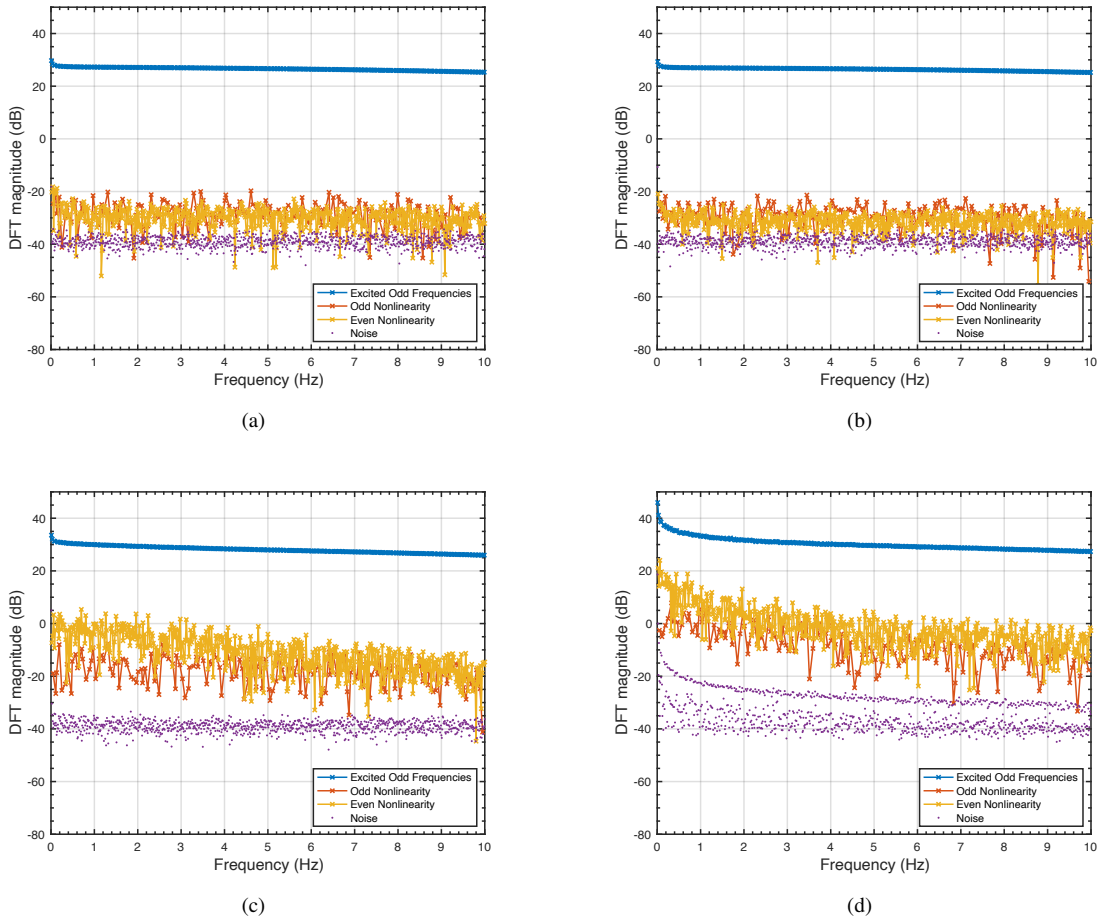

Fig. 6. Full cell voltage output spectrum at 1.5 C-rate while SoC is: (a) 90% SoC, (b) 50% SoC, (c) 10% SoC and (d) 2% SoC

According to the nature of non-linear systems, if the excitation input is designed to only contain energy at the excited odd frequencies, the energy appearing at the suppressed frequencies in the output spectrum, termed as non-linear distortion, is caused by non-linear behaviors. And the magnitude of non-linear distortion is related to the strength of non-linear behaviors [26, 36, 39]. Therefore, the upward shifting of non-linear distortions indicates that the battery behavior gradually changes from a linear to non-linear behavior. Furthermore, the magnitude of the even non-linearity is greater than odd at the low frequency range, especially at the higher current levels. This shows the dominance of the even non-linearity at the characteristic low frequency range of diffusion process, which is consistent with [26]. Wolff et al also concluded that the even harmonic is more sensitive than odd harmonic for diffusion processes based on simulation results [18].

From these results it can be concluded that the significant non-linearity occurs at the lowest SoC level and the highest current level. And, the non-linear distortion in low frequency range varies significantly at various operating conditions, while the even non-linearity is dominant in the lithium-ion battery. From the aspect of electrochemical

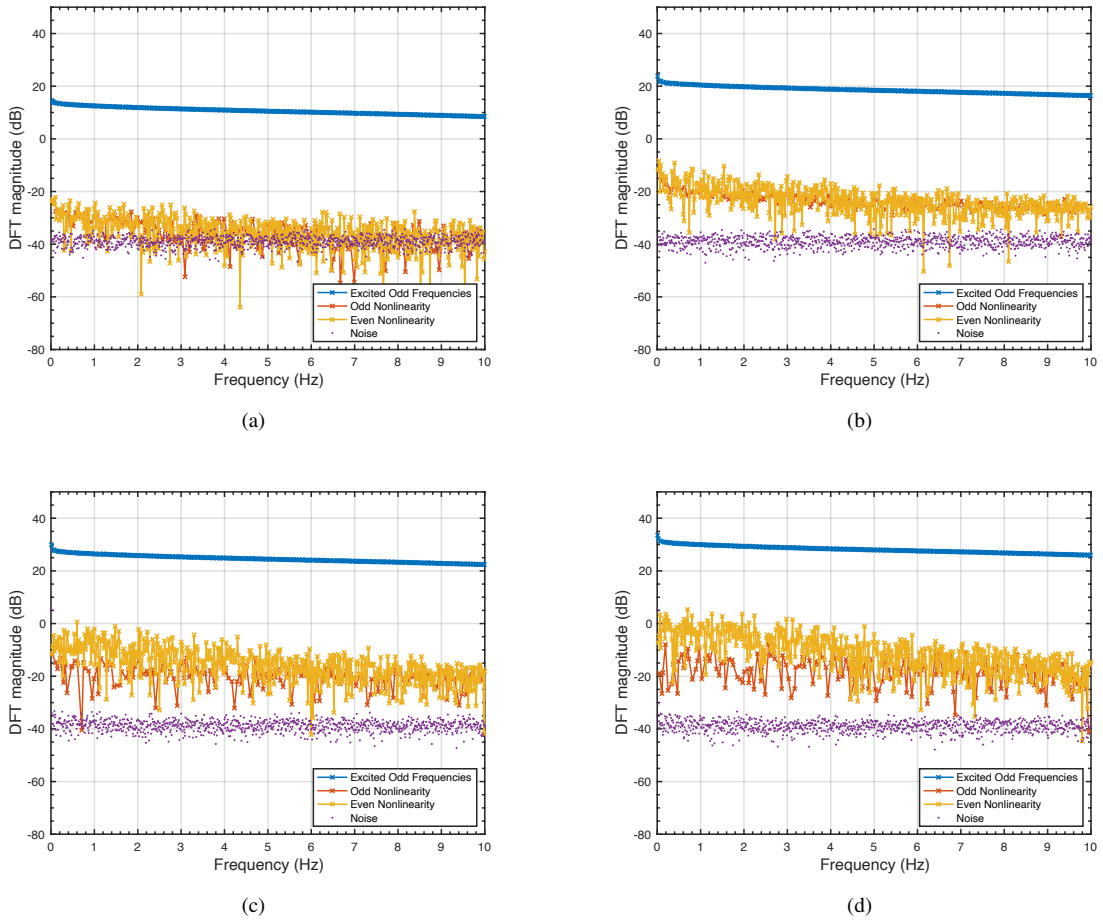

Fig. 7. Full cell voltage output spectrum at 10% SoC while current signal is: (a) 0.2C, (b) 0.5C, (c) 1.0C and (d) 1.5C

reaction processes, since the low frequency range mainly reflects the dynamic response of solid diffusion processes, the results reveals that the diffusion process of solid particles is more sensitive to SoC and excitation current.

5.2.2. Dominant non-linear distortion Analysis - Electrodes

Due to the EL-Cell three-electrodes cell configuration, the voltage response of the anode and cathode is also recorded while the full cell data is collected. Applying the same theory as in last section, the output spectrum of the cathode and anode can be plotted to evaluate which of the electrodes contribute to the non-linearity that was identified at the full cell level. In order to determine the dominant non-linear contributor of the individual electrodes, the odd and even non-linear distortions of the cathode and anode at two extreme operating conditions (90% SoC/0.2 C-rate and 10% SoC/1.5 C-rate) are also extracted and plotted in Fig.8. Corresponding to the conclusion of the previous section there is a low level of non-linearity at high SoC and low C-rate (90% SoC 0.2C Fig.8(a) and Fig.8(b)) and a high non-linearity case when at low SoC and high C-rate (10% SoC 1.5C Fig.8(c) and Fig.8(d)). In Fig.8(a) and Fig.8(b),

both cathode and anode non-linearity levels are around the full cell level, regardless of even or odd. In contrast, the low SoC and high current level (10% SoC/1.5 C-rate) shows a noticeable level of non-linear distortion in Fig.8(c) and Fig.8(d). It's clear that the cathode is the major contributor towards the full cell non-linearity, since both odd and even non-linear distortions of the cathode almost overlap the full cell distortion level. Furthermore, the magnitude of the cathode even distortion is around 20 dB larger than the anode even distortion and the odd distortions are around 15 dB higher than the anode. A possible explanation is that, at a low SoC level (10% SoC), the anode is mostly delithiated and the remaining few lithium ions do not excite significant non-linearity. However, there is a special case at 2% SoC that the anode non-linearities start to dominate in the full cell at the high C-rate currents, which will be discussed in Section 5.5.

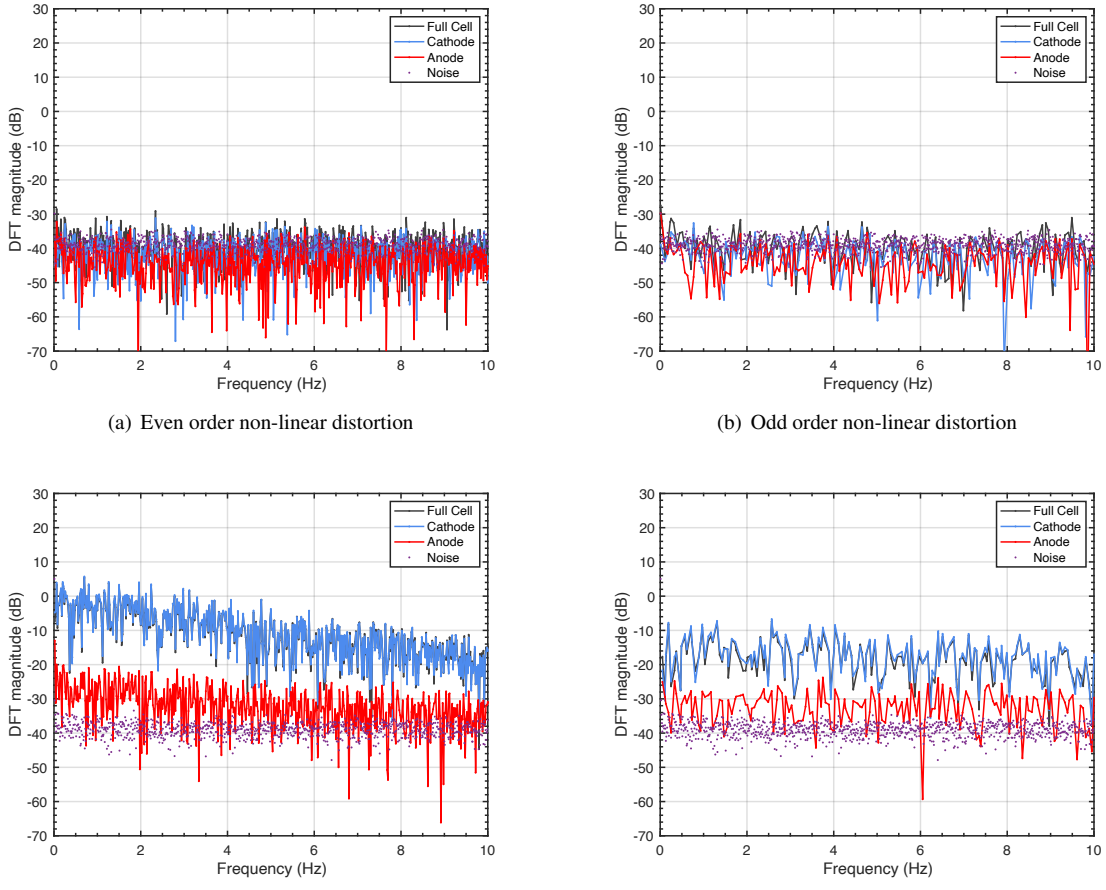

(a) Even order non-linear distortion

(b) Odd order non-linear distortion

(c) Even order non-linear distortion

(d) Odd order non-linear distortion

Fig. 8. Even and odd non-linear distortions of EL-Cell at: (a) Even non-linear distortion at 90% SoC 0.2C-rate, (b) Odd non-linear distortion at 90% SoC 0.2C-rate, (c) Even non-linear distortion at 10% SoC 1.5C-rate, and (d) Odd non-linear distortion at 10% SoC 1.5C-rate

In conclusion, the even non-linear distortions from the cathode was identified as the major contributor towards the full cell total non-linearity. Therefore, the full cell dynamic behavior can be better understood via investigating the

variation of cathode even non-linearity. In the following sections, the SoC dependency and C-rate dependency of the even non-linear distortion of the cathode will be studied.

5.3. SoC dependency of cathode even non-linearity

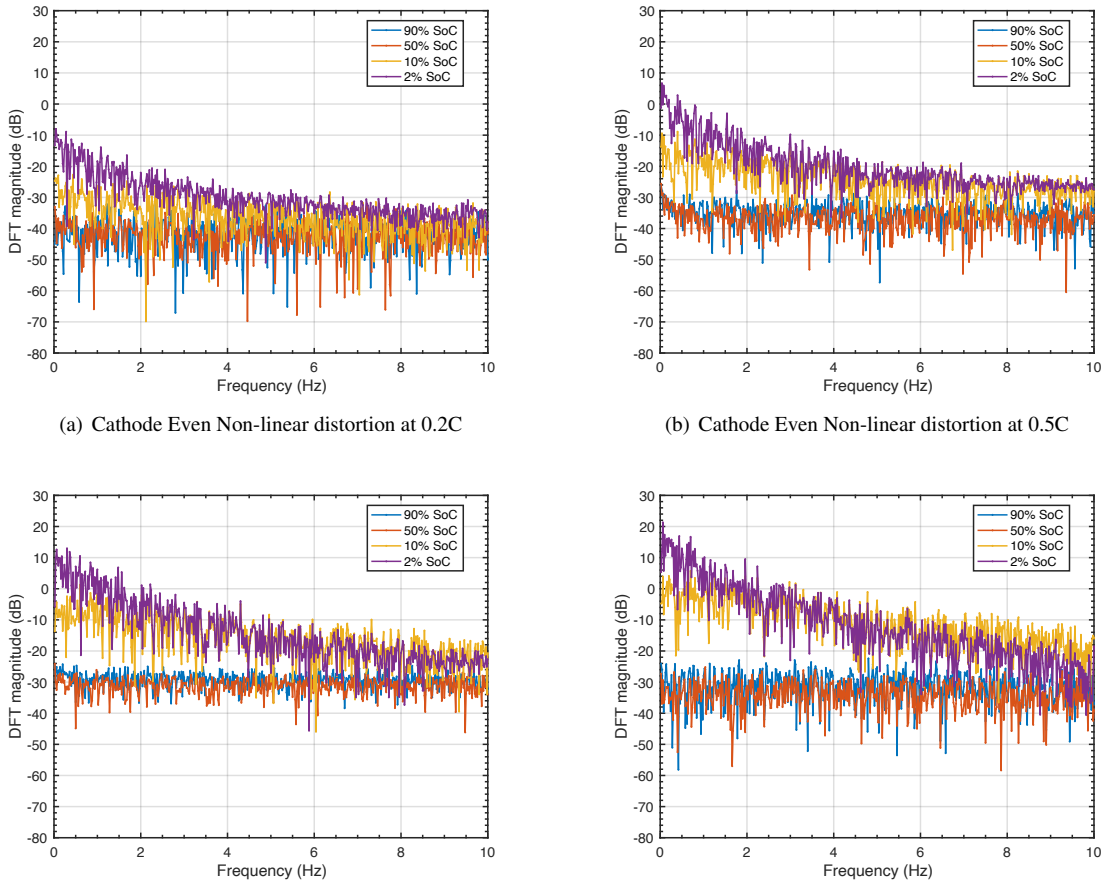

(a) Cathode Even Non-linear distortion at 0.2C

(b) Cathode Even Non-linear distortion at 0.5C

(c) Cathode Even Non-linear distortion at 1.0C

(d) Cathode Even Non-linear distortion at 1.5C

Fig. 9. Cathode even non-linear distortions at various SoC levels while current signal is: (a) 0.2C, (b) 0.5C, (c) 1.0C and (d) 1.5C

Fig.9 shows the even non-linear distortion of the cathode at various SoC levels when different C-rate current signals were applied. As the SoC level decreases, the magnitude of non-linear distortion significantly increases. For example, in Fig.9(d), the cathode even non-linear distortion at 10 mHz raises from −30 dB to around 15 dB when the SoC level decreases from 50% to 2%. Nevertheless, from 90% to 50% SoC, no noticeable increase is seen in the level of non-linear distortion. Referring to [18], the exponential shape curve is also obtained at low frequency range by simulating the model of Fick's law for diffusion process. Therefore, the steeper slope of non-linear distortion level in low frequency range indicates that the intensity of the diffusion process depends on the SoC level of a lithium-ion battery. From the minimum frequency 10 mHz to the maximum frequency 10 Hz, the magnitude difference of cathode

non-linear distortion levels between 2% SoC and 90% SoC decreases from 45 dB to around 5 dB correspondingly. It suggests that the electrodes reactions, which is commonly interpreted by Butler-Volmer kinetics, is not as susceptible to the non-linear distortions at various SoC levels as much as the diffusion process.

It is also observed (in Fig.12) that the cathode even non-linear distortion at 2% and 10% SoC substantially increases when the excitation signal C-rate level enhances. However when at 50% SoC and 90%, the level of non-linearity is low and fairly constant across the frequency range with no clear separation at all four C-rate levels. This indicates that the non-linear behavior at high SoC levels is not susceptible to the amplitude of the excitation current as at low SoC levels. This is investigated further in the next section.

5.4. C-rate dependency of cathode even non-linearity

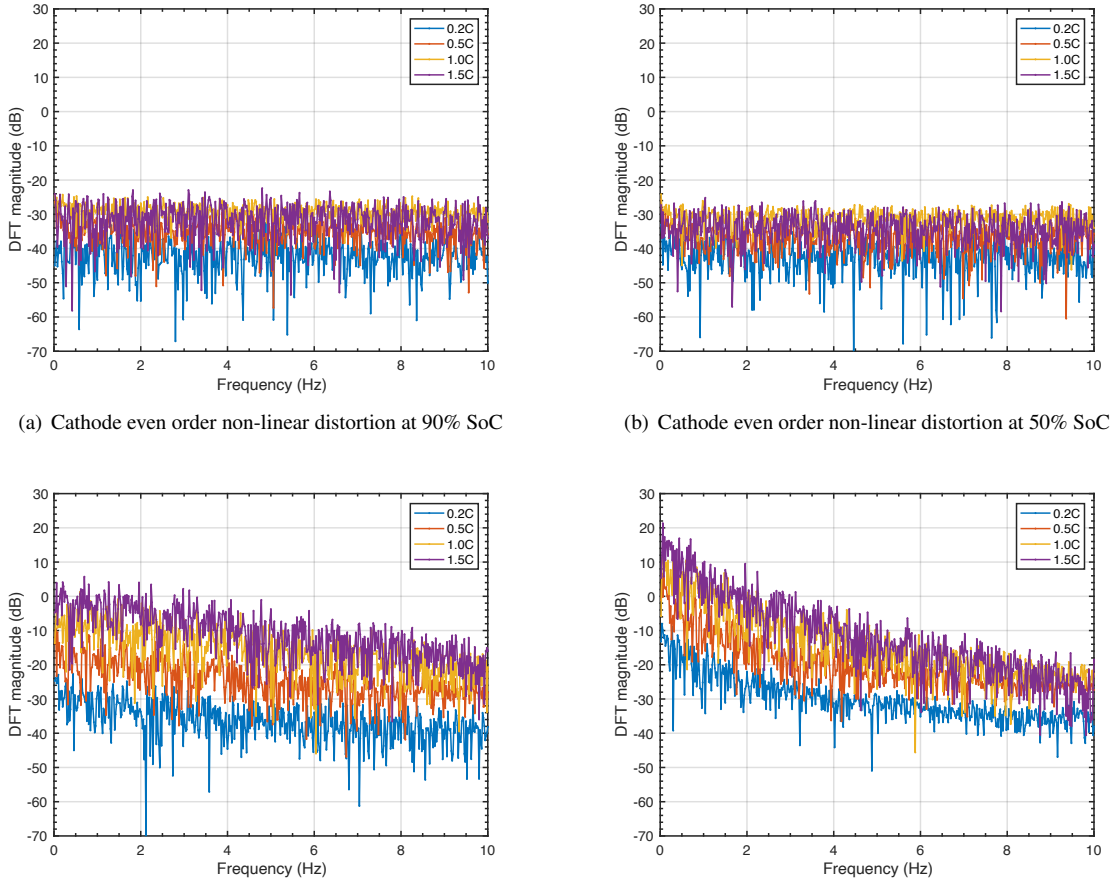

(a) Cathode even order non-linear distortion at 90% SoC

(b) Cathode even order non-linear distortion at 50% SoC

(c) Cathode even order non-linear distortion at 10% SoC

(d) Cathode even order non-linear distortion at 2% SoC

Fig. 10. Cathode even non-linear distortions at various C-rates while SoC is: (a) 90% SoC, (b) 50% SoC, (c) 10% SoC and (d) 2% SoC

As a lithium ion battery exhibits different intensities of non-linearity at various C-rates, in Fig.10, the cathode even non-linear distortions are shown according to each SoC level to investigate the C-rate dependency. Consistent with the

phenomenon in the last section, the non-linear distortion at the high SoC levels are similar in magnitude irrespective of the C-rates, as seen in Fig.10(a) and Fig.10(b), which indicates both reaction process and diffusion process are not sensitive to different excitation current levels at higher SoC. At lower SoC levels (Fig. 10(c) and Fig.10(d)), the even non-linear distortion of diffusion process gradually increases in the lower frequency range as the C-rate increases, which indicates the presence of possible non-linear diffusion processes at low SoC regions when the C-rate increases.

However, Fig.9(d) shows an anomaly that the non-linear distortion level of 2% SoC is lower than 10% over the medium frequency range at 1.5C current input. This phenomena does not conform to theory that a higher C-rate excites larger non-linear distortion, therefore, in the next section, the special case of dynamics response at 2% SoC will be analysed.

5.5. Special Case: frequency response at 2% SoC

It's supposed that the 2% SoC dynamics are different due to the extreme distribution of lithium ion concentration between cathode and anode. Therefore, to investigate this behavior, the even and odd non-linear distortions of the cathode and anode at 10% and 2% SoC levels were plotted in Fig.11. Overall, the even non-linear distortions are still the dominant contributor in either the anode or cathode and is about 10 dB larger than the magnitude of odd non-linear distortions. However, Fig.11(c) shows that the major contributor towards the even non-linear distortion shifted from the cathode to anode around 2 Hz at low SoC (2%), which means the dynamics of the anode changed at the low SoC conditions.

Focusing on this low SoC condition, the even and odd non-linear distortion at 2% SoC for different C-rate levels are shown in Fig.12 and Fig.13, respectively. Consistently, the cathode remains as the dominant contributor towards the odd non-linear distortion between individual electrodes at every current level (see Fig.13). On the contrary, the even non-linearity from the anode increased dramatically and became dominant with the increase in C-rate. The variation of the cathode even non-linear distortion magnitude increased by around 20 dB from 0.5 C-rate to 2.0 C-rate, however, there was almost a 30 dB magnitude rise for the anode. Referring to [18], the simulation results show that, as the symmetry factor α in Butler-Volmer kinetics varies, the non-linear distortion of even harmonic is significantly excited. Therefore, at 2.0% SoC level, the low lithium ion concentration in anode and high current level input may lead to changes of the symmetry factor α related components, such that the even non-linearity of the anode increases greatly. Hence, when analysing non-linear behavior, the 2% SoC level should be paid attention as a special case.

6. Conclusion

In this study, the non-linearity of NMC based lithium-ion EL-Cells have been characterized using multisine signals over a wide range of excitation amplitudes and SoC conditions. The random phase multisines with all even harmonics and several odd harmonics suppressed were used as an excitation input current signal, which leads to the faster characterization procedure of the battery non-linearity than conventional techniques. The dynamic response analysis,

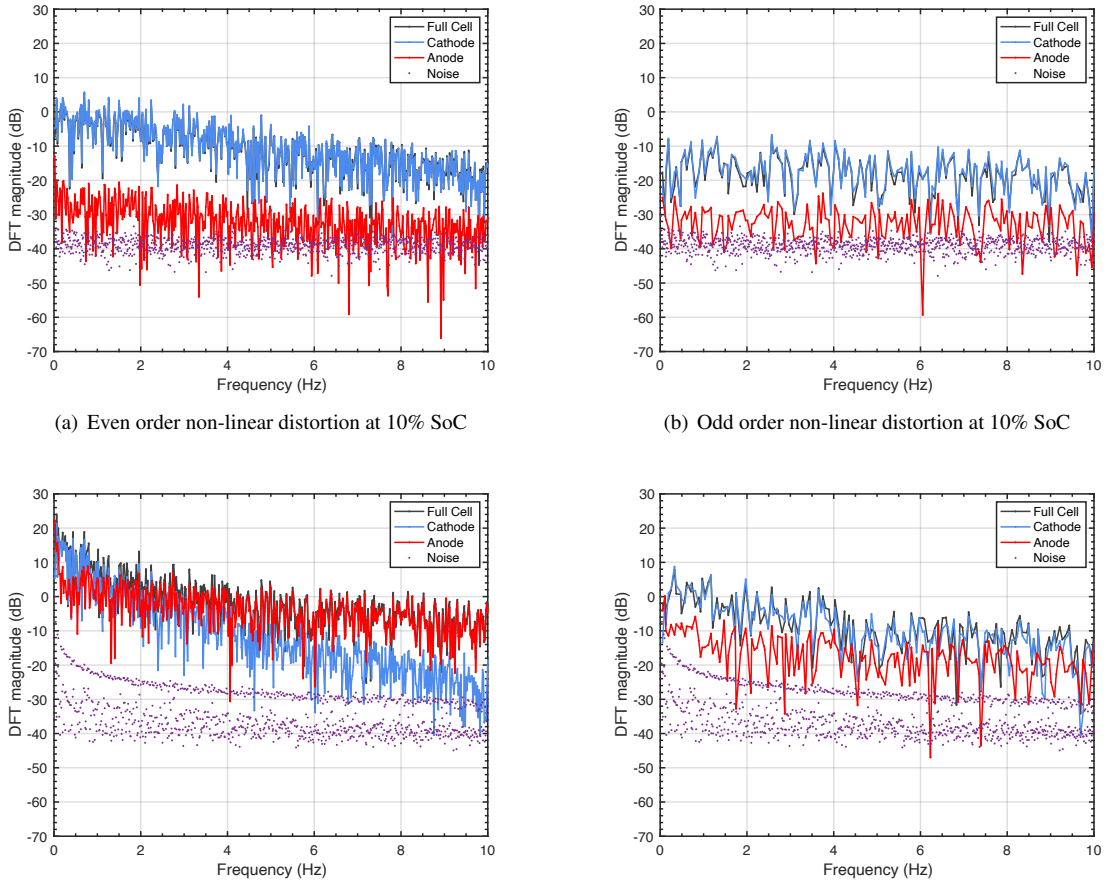

(a) Even order non-linear distortion at 10% SoC

(b) Odd order non-linear distortion at 10% SoC

(c) Even order non-linear distortion at 2% SoC

(d) Odd order non-linear distortion at 2% SoC

Fig. 11. Even and odd non-linear distortions of EL-Cell at 1.5 C-rate while at : (a), (b) 10% SoC and (c), (d) 2% SoC

which focused on the diffusion process and electrode reaction of cathode, anode and full cell, were performed by analysing the non-excited harmonics in the voltage output spectrum, which provides valuable information for battery system modelling to increase accuracy. First, it can be concluded that non-linear distortions are very low at high SoCs (>10%), as such the battery current voltage relationship is behaving linearly in these regions and a linear model will suffice. Moreover, at low SoCs ($\leqslant$ 10%) the non-linear distortion significantly increase, and the even non-linearity originating from the cathode was concluded as the dominant non-linear contributor of a lithium-ion battery. The possible sources for this non-linearity include open circuit potential (OCP) change that occurs at low SoC for the cathode, the other potential possibility is that the Butler-Volmer kinetic and mass transport due to the high lithium ion concentration in the cathode. Additionally, the dominance of the even non-linear distortion at even harmonics indicates that an even order non-linear characteristic function is required for modelling non-linear behaviors of a lithium-ion battery, nevertheless, the relationship between odd/even harmonics and electrochemical processes is still an open question which is worth exploring. Last but not the least, a special case is shown where the dynamics of the anode

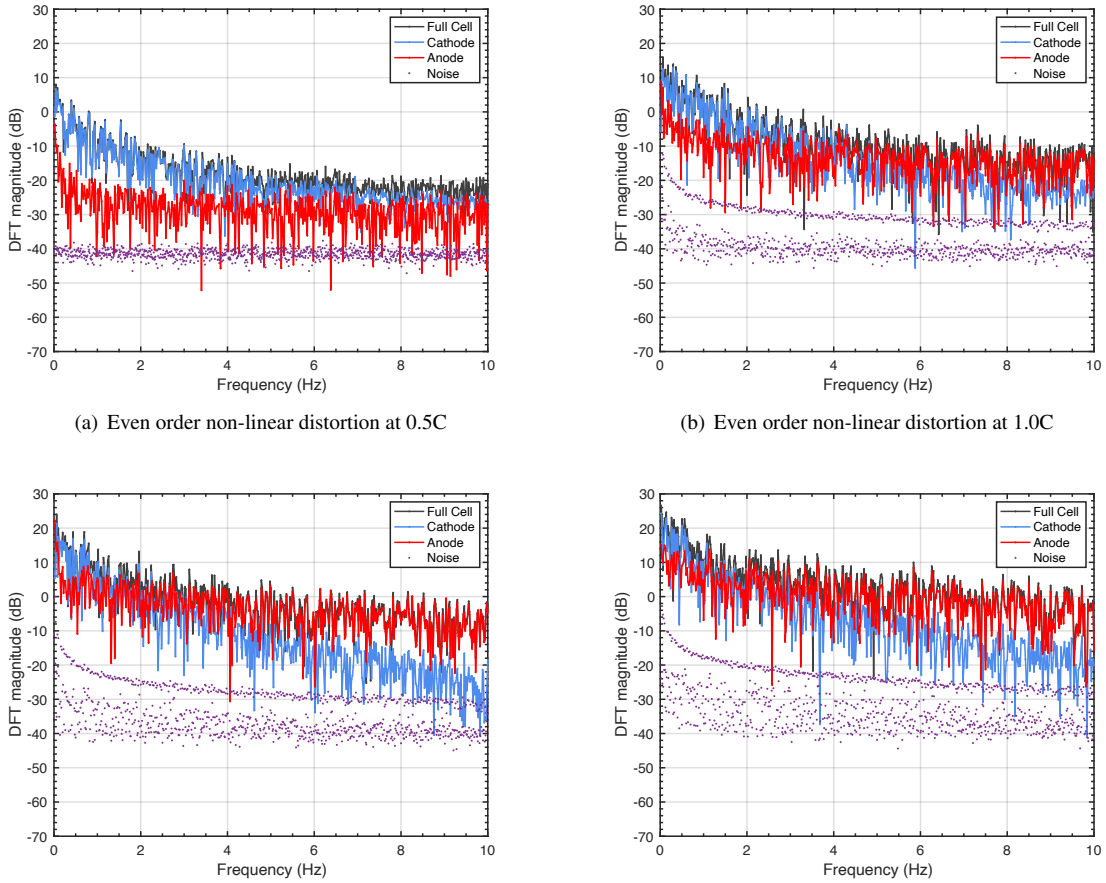

(a) Even order non-linear distortion at 0.5C

(b) Even order non-linear distortion at 1.0C

(c) Even order non-linear distortion at 1.5C

(d) Even order non-linear distortion at 2.0C

Fig. 12. Even non-linear distortions of EL-Cell at 2.0% SoC while at : (a) 0.5C, (b) 1.0C, (c) 1.5C and (d) 2.0C

change at 2% SoC and contribute significant even non-linear distortion. The open circuit potential is an important factor for this phenomena, however, at the moment, the contribution of open circuit potential and the other non-linear behaviors to the non-linearity of the system cannot be clearly distinguished. Therefore, further investigations are needed to decouple the contribution of each electrochemical behavior towards battery system non-linearity.

If a sophisticated model can be developed to account for these non-linear distortions then the model accuracy at low SoCs can be improved. From the perspective of frequency domain system identification theory, the non-linearity of the battery has to be captured and quantized in advance, and then, according to the characterised level of the non-linearity, it can be accounted via an appropriate non-linear function (e.g. sigmoid, neural nets or polynomials) and added into equivalent circuit model (ECM) to improve model accuracy (such examples at a full cell level can be found in [24] and [40]). Meanwhile, the model will have the advantage to separate the voltage response of each electrodes from a three-electrode cell configuration. Then it will be validated with a real EL-Cell and a related commercial cell to evaluate the accuracy at low SoC levels.

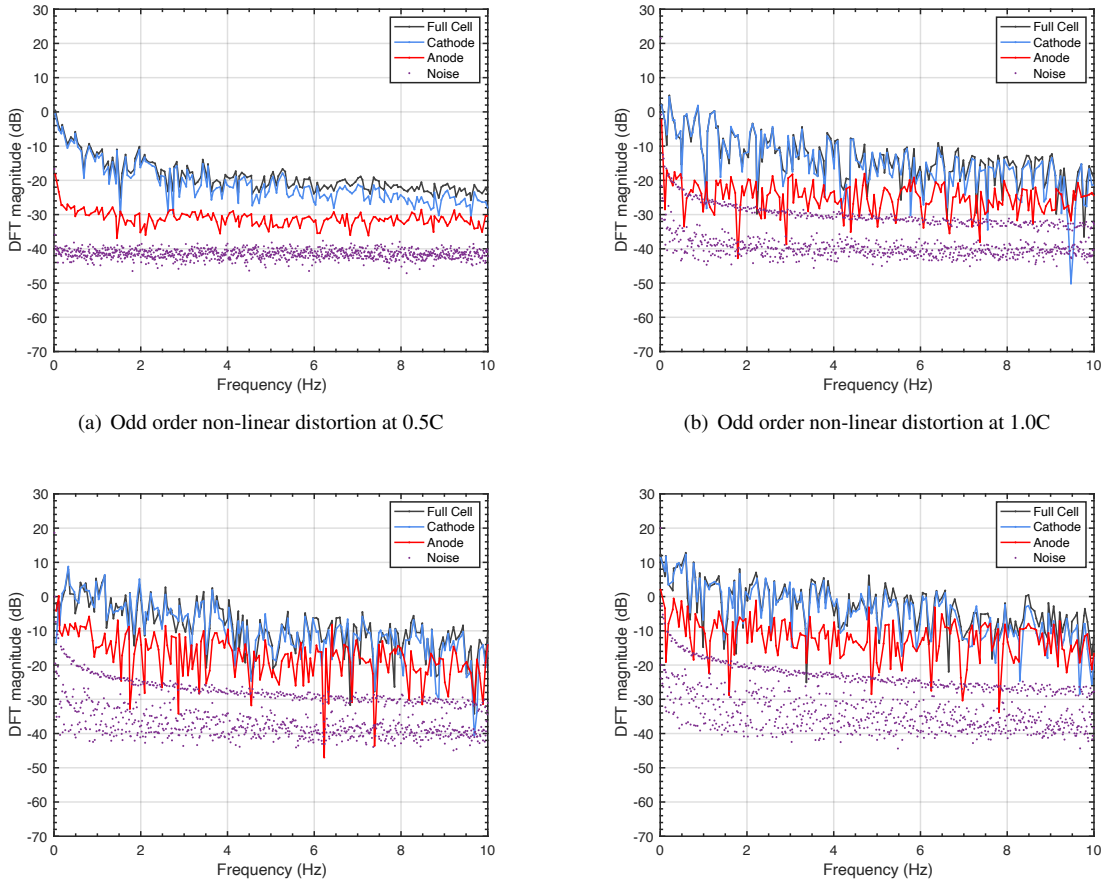

(a) Odd order non-linear distortion at 0.5C

(b) Odd order non-linear distortion at 1.0C

(c) Odd order non-linear distortion at 1.5C

(d) Odd order non-linear distortion at 2.0C

Fig. 13. Odd non-linear distortions of EL-Cell at 2.0% SoC while C-rate at : (a) 0.5C, (b) 1.0C, (c) 1.5C and (d) 2.0C

Acknowledgement

The research presented within this paper is supported by WMG, University of Warwick (09ESWM21) and Institute of Digital Engineering (IDE) under a grant for Virtually Connected Hybrid Vehicle project.

References

[1] G. L. Plett, Extended kalman filtering for battery management systems of lipb-based hev battery packs: Part 3. state and parameter estimation, Journal of Power sources 134 (2) (2004) 277–292.

[2] D. Di Domenico, A. Stefanopoulou, G. Fiengo, Lithium-ion battery state of charge and critical surface charge estimation using an electrochemical model-based extended kalman filter, Journal of dynamic systems, measurement, and control 132 (6).

[3] G. L. Plett, Battery management systems, Volume II: Equivalent-circuit methods, Vol. 2, Artech House, 2015.

[4] R. Xiong, J. Cao, Q. Yu, H. He, F. Sun, Critical review on the battery state of charge estimation methods for electric vehicles, Ieee Access 6 (2017) 1832–1843.

[5] R. Xiong, L. Li, J. Tian, Towards a smarter battery management system: A critical review on battery state of health monitoring methods, Journal of Power Sources 405 (2018) 18–29.

[6] Q. Ouyang, Z. Wang, K. Liu, G. Xu, Y. Li, Optimal charging control for lithium-ion battery packs: A distributed average tracking approach, IEEE Transactions on Industrial Informatics.

[7] F. Feng, S. Teng, K. Liu, J. Xie, Y. Xie, B. Liu, K. Li, Co-estimation of lithium-ion battery state of charge and state of temperature based on a hybrid electrochemical-thermal-neural-network model, Journal of Power Sources 455 (2020) 227935.

[8] M. Ouyang, G. Liu, L. Lu, J. Li, X. Han, Enhancing the estimation accuracy in low state-of-charge area: A novel onboard battery model through surface state of charge determination, Journal of Power Sources 270 (2014) 221–237.

[9] X. Hu, S. Li, H. Peng, A comparative study of equivalent circuit models for Li-ion batteries, Journal of Power Sources 198 (2012) 359–367. doi:10.1016/j.jpowsour.2011.10.013.

[10] R. Relan, Y. Firouz, J.-M. Timmermans, J. Schoukens, Data-driven nonlinear identification of li-ion battery based on a frequency domain nonparametric analysis, IEEE Transactions on Control Systems Technology 25 (5) (2016) 1825–1832.

[11] S. Nejad, D. Gladwin, D. Stone, A systematic review of lumped-parameter equivalent circuit models for real-time estimation of lithium-ion battery states, Journal of Power Sources 316 (2016) 183–196.

[12] F. Marra, G. Y. Yang, C. Træholt, E. Larsen, C. N. Rasmussen, S. You, Demand profile study of battery electric vehicle under different charging options, in: 2012 IEEE Power and Energy Society General Meeting, IEEE, 2012, pp. 1–7.

[13] T. F. Fuller, M. Doyle, J. Newman, Simulation and optimization of the dual lithium ion insertion cell, Journal of the Electrochemical Society 141 (1) (1994) 1–10.

[14] A. Jokar, B. Rajabloo, M. Désilets, M. Lacroix, Review of simplified Pseudo-two-Dimensional models of lithium-ion batteries, Journal of Power Sources 327 (2016) 44–55. doi:10.1016/j.jpowsour.2016.07.036.

[15] S. J. Moura, F. B. Argomedo, R. Klein, A. Mirtabatabaei, M. Krstic, Battery state estimation for a single particle model with electrolyte dynamics, IEEE Transactions on Control Systems Technology 25 (2) (2017) 453–468.

[16] J. Newman, K. E. Thomas-Alyea, Electrochemical systems, John Wiley & Sons, 2012.

[17] C. D. Rahn, C.-Y. Wang, Battery systems engineering, John Wiley & Sons, 2013.

[18] N. Wolff, N. Harting, F. Röder, M. Heinrich, U. Krewer, Understanding nonlinearity in electrochemical systems, The European Physical Journal Special Topics 227 (18) (2019) 2617–2640.

[19] C. Pastor-Fernández, K. Uddin, G. H. Chouchelamane, W. D. Widanage, J. Marco, A Comparison between Electrochemical Impedance Spectroscopy and Incremental Capacity-Differential Voltage as Li-ion Diagnostic Techniques to Identify and Quantify the Effects of Degradation Modes within Battery Management Systems, Journal of Power Sources 360 (2017) 301–318. doi:10.1016/j.jpowsour.2017.03.042.

[20] N. Harting, N. Wolff, F. Röder, U. Krewer, Nonlinear Frequency Response Analysis (NFRA) of Lithium-Ion Batteries, Electrochimica Acta 248 (2017) 133–139. doi:10.1016/j.electacta.2017.04.037.

[21] A. Barai, K. Uddin, M. Dubarry, L. Somerville, A. McGordon, P. Jennings, I. Bloom, A comparison of methodologies for the non-invasive characterisation of commercial Li-ion cells, Progress in Energy and Combustion Science 72 (2019) 1–31. doi:10.1016/j.pecs.2019.01.001.

[22] H. Zappen, F. Ringbeck, D. U. Sauer, Application of time-resolved multi-sine impedance spectroscopy for lithium-ion battery characterization, Batteries 4 (4) (2018) 64.

[23] W. D. Widanage, A. Barai, G. H. Chouchelamane, K. Uddin, A. Mcgordon, J. Marco, P. Jennings, Design and use of multisine signals for Li-ion battery equivalent circuit modelling. Part 1: Signal design, Journal of Power Sources 324 (2016) 70–78. doi:10.1016/j.jpowsour.2016.05.015.

[24] W. D. Widanage, A. Barai, G. H. Chouchelamane, K. Uddin, A. McGordon, J. Marco, P. Jennings, Design and use of multisine signals for Li-ion battery equivalent circuit modelling. Part 2: Model estimation, Journal of Power Sources 324 (2016) 61–69. doi:10.1016/j.jpowsour.2016.05.014.

[25] Y. Firouz, N. Omar, S. Goutam, J. Timmermans, P. den Bossche, J. Mierlo, Measuring and analysis of nonlinear characterization of lithium-ion

batteries using multisin excitation signal, World Electric Vehicle Journal 8 (2) (2016) 362–370.

[26] Y. Firouz, R. Relan, J. M. Timmermans, N. Omar, P. Van den Bossche, J. Van Mierlo, Advanced lithium ion battery modeling and nonlinear analysis based on robust method in frequency domain: Nonlinear characterization and non-parametric modeling, Energy 106 (2016) 602–617. doi:10.1016/j.energy.2016.03.028.

[27] A. Nickol, T. Schied, C. Heubner, M. Schneider, A. Michaelis, M. Bobeth, G. Cuniberti, Gitt analysis of lithium insertion cathodes for determining the lithium diffusion coefficient at low temperature: Challenges and pitfalls, Journal of the Electrochemical Society.

[28] S. S. Zhang, Is li/graphite half-cell suitable for evaluating lithiation rate capability of graphite electrode?, Journal of the Electrochemical Society.

[29] E. McTurk, T. Amietszajew, J. Fleming, R. Bhagat, Thermo-electrochemical instrumentation of cylindrical li-ion cells, Journal of Power Sources 379 (2018) 309–316.

[30] S. P. Rangarajan, Y. Barsukov, P. P. Mukherjee, In operando impedance based diagnostics of electrode kinetics in li-ion pouch cells, Journal of The Electrochemical Society 166 (10) (2019) A2131.

[31] D. Juarez-Robles, C.-F. Chen, Y. Barsukov, P. P. Mukherjee, Impedance evolution characteristics in lithium-ion batteries, Journal of The Electrochemical Society 164 (4) (2017) A837.

[32] M. Wünsch, R. Füßler, D. U. Sauer, Metrological examination of an impedance model for a porous electrode in cyclic aging using a 3-electrode lithium-ion cell with NMC111 — Graphite, Journal of Energy Storage 20 (2018) 196–203. doi:10.1016/j.est.2018.09.010.

[33] Q. Gao, H. Dai, X. Wei, B. Jiang, Impedance modeling and aging research of the lithium-ion batteries using the EIS technique, SAE Technical Papers 2019-April (April). doi:10.4271/2019-01-0596.

[34] J. Costard, M. Ender, M. Weiss, E. Ivers-Tiffée, Three-electrode setups for lithium-ion batteries, Journal of The Electrochemical Society 164 (2) (2016) A80.

[35] C.-H. Chen, F. B. Planella, K. O'Regan, D. E. Gastol, W. D. Widanage, E. Kendrick, Development of experimental techniques for parameterization of multi-scale lithium-ion battery models, Journal of the Electrochemical Society.

[36] R. Pintelon, J. Schoukens, System Identification: A Frequency Domain Approach, Second Edition, John Wiley and Sons, 2012. doi:10.1002/9781118287422.

[37] X.-G. Yang, S. Ge, T. Liu, Y. Leng, C.-Y. Wang, A look into the voltage plateau signal for detection and quantification of lithium plating in lithium-ion cells, Journal of Power Sources 395 (2018) 251–261.

[38] R. Xiong, J. Cao, Q. Yu, H. He, F. Sun, Critical Review on the Battery State of Charge Estimation Methods for Electric Vehicles, IEEE Access 6 (2017) 1832–1843. doi:10.1109/ACCESS.2017.2780258.

[39] J. Schoukens, R. Pintelon, Y. Rolain, Mastering system identification in 100 exercises, John Wiley & Sons, 2012.

[40] Y. Firouz, S. Goutam, M. C. Soult, A. Mohammadi, J. Van Mierlo, P. Van den Bossche, Block-oriented system identification for nonlinear modeling of all-solid-state li-ion battery technology, Journal of Energy Storage 28 (2020) 101184.